Journal of Molecular Structure 1142 (2017) 40–47

Contents lists available at ScienceDirect

Journal of Molecular Structure

journal homepage: http://www.elsevier.com/locate/molstruc

New mixed ligand cobalt(II/III) complexes based on the drug sodium valproate and bioactive nitrogen-donor ligands. Synthesis, structure and biological properties

Hijazi Abu Ali*, [1], Amani Abu Shamma [1], Shayma Kamel [1]

Department of Chemistry, Birzeit University, West Bank, Palestine

ARTICLE INFO

Article history:
Received 29 August 2016
Received in revised form
12 April 2017
Accepted 12 April 2017

Keywords:
Cobalt valproate complexes
Nitrogen donor ligands
Valproate coordination modes

ABSTRACT

New cobalt valproate complexes with different nitrogen based ligands were synthesized and characterized using various techniques such as IR, UV–Vis, single crystal X-ray diffraction as well as other physical properties. The general formula of the prepared complexes is $[Co_n(valp)_m(L)_z]$, (n = 1, 2 …; m = 1, 2, …; Z = 1, 2 …). The complexes $[Co_2(valp)_4]$ **(1)**, $[Co(valp)_2(2\text{-ampy})_2]$ **(2)** and $[Co_2(valp)_4(quin)_2]$ **(3)** showed different carboxylate coordination modes. The crystal structures of the complexes **2** and **3** were determined using single crystal X-ray diffraction. Kinetic studies of hydrolysis reactions of BNPP [*bis*-(p-nitrophenyl)phosphate] with complexes **2** and **3** were performed. The hydrolysis rate of BNPP was studied at different temperatures, pH and concentrations by UV–Vis spectrophotometric method. The results showed that the hydrolysis rate of BNPP was 7.70×10^2 L mol^{-1} s^{-1} for (**3**) and 2.60×10^{-1} L mol^{-1} s^{-1} for (**2**).

1. Introduction

Co^{3+} ion can be found in different biological systems such as vitamin B12 (cobalamin) which is a cofactor for many enzymes like methyl transferases, and isomerases and it's a key important in biological system in the formation of blood and the normal functioning of the nervous system and brain [1–5].

Cobalt ion has been widely used in therapeutic drugs because it has a variety of geometries, coordination numbers and oxidation states [6]. Moreover, it is less toxic than other metals like platinum [5]. Among the most common ligands which were used to prepare Co complexes as anticancer agents are phenanthroline and tridentate N,O-donor ligands [7].

Nitrogen based ligands can be used in the synthesis and design of compounds in biological, chemotherapy and pharmacological applications such as anti-rheumatics and anti-histamines [8,9]. The ligands 2-amino pyridine and quinoline exhibit anti-tumor, anti-bacterial, anti-viral, anti-malarial and anti-fungal activities [10–12].

Valproic acid (2-propylvaleric or *n*-dipropylacetic or 2-propylpentanoic acid) is a short chain fatty acid which is a carboxylic acid [13–17]. Recently, valproic acid has a wide range clinical uses such as antibiotic drugs for treatment of many diseases such as epilepsy and bipolar disorder [13,15,17]. But it causes many side effects in human organisms such as gastrointestinal disturbances and headache. Valproate complexation with metal may reduce these side effects and enhance the biological activity [15,17,18].

The transition metal with carboxylate complexes are used in biological systems and industrial applications such as dirheniu-m(III) dichlorotetraisobutyrate which inhibits cancer cells while dirhodium(II) tetraacetate which is used as catalyst [19]. There are many examples of metal valproate complexes such as copper, cadmium(II), cobalt(II), zinc(II) and manganese(II) [20–23]. Tabrizi and McArdle have studied cadmium (II), cobalt(II) and manganese(II) valproate with 1,10-phenanthroline and imidazole. These complexes were synthesized and characterized by using various techniques. The complexes were tested for their biological activities such as anti-bacterial activity by using agar diffusion method and anti-cancer cells [23].

The hydrolytic cleavage of phosphatediester bond is very difficult to occur, but the hydrolysis may be enhanced by using an artificial catalyst which may be organic or inorganic compound.

* Corresponding author. Department of Chemistry, Birzeit University, P.O. Box 14, West Bank, Palestine.
E-mail addresses: habuali@birzeit.edu, habuali1@yahoo.com (H. Abu Ali).
[1] These authors have contributed equally to this work.

http://dx.doi.org/10.1016/j.molstruc.2017.04.048
0022-2860/

The temperature, structure of the catalyst and the pH value are factors affecting the hydrolysis of phosphatediester bond [24,25]. The hydrolysis of BNPP is very important in environmental, industrial and biological applications [26,27].

2. Experimental

2.1. Chemicals, materials and biological species

All reagents, chemicals and solvents were purchased from commercial sources and were used without further purification.

2.2. Physical measurements

Melting points were measured by using Electrothermal melting point apparatus. IR spectra of cobalt complexes were taken on a Bruker Tensor II as KBr pellets in the region 200–4000 cm^{-1}. UV–Vis spectra in MeOH solvent in the region 200–800 nm were determined by using Agilent 8453 photodiode array (PDA) spectrophotometer. The magnetic susceptibility measurements of the powder solid complexes were determined by magnetic susceptibility, $HgCo(NSC)_4$ complex (mercury cobalt-thiocyanate) was used as a standard complex.

2.3. Synthesis of cobalt valporate complexes

All cobalt valproate complexes were prepared at room temperature (RT).

2.3.1. Synthesis of cobalt valporate $[Co_2(valp)_4]$ (**1**)

Sodium valproate (2.00 g, 12.1 mmol) in water was slowly added to a stirred aqueous solution of $CoCl_2 \cdot 6H_2O$ (1.42 g, 6.00 mmol), then the formed purple solid was filtered from aqueous solution, washed with cold water and air dried. The complex was characterized by using IR-spectroscopy, UV-spectroscopy.

Yield = 86.50%; m. p = 58 °C; IR (KBr, cm^{-1}): 2959, 2872, 1556, 1450, 1419, 1330, 753, 469; UV–Vis (MeOH, λ (nm) (ε/$Lmol^{-1}cm^{-1}$)): 270 (7576.5), 492 (43.6).

2.3.2. Synthesis of cobalt valporate 2-aminopyridine complex $[Co(valp)_2(2\text{-}ampy)_2]$ (**2**)

2-ampy (0.96 g, 10.2 mmol) in MeOH was slowly added to a stirred MeOH solution of complex **1** (0.93 g, 2.6 mmol), the solution was then stirred for 3.5 h, the solvent was evaporated and a pink precipitate was obtained. The complex was characterized by using IR-spectroscopy, UV-spectroscopy, magnetic moment and single crystal X-ray diffraction. Recrystallization from methanol produced suitable crystals for X-ray structure determination.

Yield = 79.85%; m. p = 121–125 °C; IR (KBr, cm^{-1}): 3413, 3331, 3080, 3070, 2959, 2930, 2870, 1651, 1565, 1495, 1448, 1329, 1270, 1226, 1156, 1113, 1066, 1003, 864, 769, 740, 657, 518, 451; UV–Vis (MeOH, λ (nm) (ε/$Lmol^{-1}cm^{-1}$)): 235 (20072), 295 (8022.1), 520 (20.2); μ_{eff} = 4.83 BM.

2.3.3. Synthesis of cobalt valporate quinoline $[Co_2(valp)_4(quin)_2]$ (**3**)

Quin (0.91 ml, 0.98 g, 7.6 mmol) was slowly added to a stirred MeOH solution of complex **1** (1.4 g, 3.8 mmol), then the solution was stirred for 5 h, the solvent was evaporated and a green precipitate was obtained. The complex was characterized by using IR-spectroscopy, UV-spectroscopy, magnetic moment and single crystal X-ray diffraction. Recrystallization from methanol produced suitable crystals for X-ray structure determination.

Yield = 26.23%; m. p = 110–111 °C; IR (KBr, cm^{-1}): 3100, 3050, 2956, 2930, 2870, 1613, 1560, 1510, 1450, 1417, 1241, 1145, 1110, 1050, 803, 782, 735, 520, 467; UV–Vis (MeOH, λ (nm) (ε/$Lmol^{-1}cm^{-1}$)): 213 (49030), 276 (9119), 366 (3.6), 520 (2.6).

2.4. X-ray crystallography

Single crystal X-ray analysis of complexes **2** and **3** were carried out by attaching single crystal to a glass fibber with epoxy glue, and then it transferred to X-ray diffractometer system (Bruker SMART APEX CCD) which is controlled by using Pentium-based PC running the SMART software package [28–30]. The diffracted graphite-monochromated (Kα radiation λ = 0.71073 Å) was detected on a phosphor screen at −44 °C and it held at 6.0 cm from the crystal. A detector array of 512 × 512 pixels (a pixel size 120 μm) was used to collect data [28]. Crystal data and structure refinements are summarized in Table 1.

2.5. Kinetic measurements of BNPP hydrolysis

The kinetic experiments were performed at different temperatures (25 °C, 37 °C and 40 °C), different pH values (7.04, 7.48 and 7.91) and different catalytic concentrations from 1×10^{-3} to 1×10^{-6} M.

HEPES buffer, (4-(2-hydroxyethyl)-1-piperazineethanesulfonic acid) was used to maintain a constant pH value. The buffer solutions were prepared by dissolving 50 μM of HEPES buffer in minimum amount of deionized water then the pH of the solution was adjusted with HCl or NaOH after that BNPP was dissolved in buffer solution and the volume of the solution was adjusted to 100 ml in the volumetric flask [31,32].

Different concentrations of the cobalt complexes were prepared in MeOH solution in order to use them as catalysis in the BNPP hydrolysis process. The rate of p-nitrophenol formation was measured using UV–vis spectrophotometer at λ = 400 nm (ε = 13400 L mol^{-1} cm^{-1}) [32–34].

The kinetic experiments were carried in triplicates by adding 1.5 ml of the cobalt complex into 1.5 ml of BNPP solution in a quartz cell at constant temp, then the solution was immediately mixed and the kinetic measurement was performed [32,33]. The initial rate (V_o) was calculated from the slope of the linear plot of p-nitrophenol concentration against time; $[(rate)_0 = (dc/dt)_0 = (dA/dt)_0/\varepsilon]$ [26].

3. Results and discussion

3.1. Synthesis of cobalt complexes

Cobalt valproate complex $[Co_2(valp)_4]$ (**1**) was prepared by adding 2 equivalents of sodium valproate to 1 equivalent of $CoCl_2$ as shown in Scheme 1. The purple solid product was obtained in 86.50% yield.

Cobalt valproate complexes **2** and **3** with different molar ratios of the N-donor ligands were synthesized as shown in Scheme 2. The physical properties of complexes **2** and **3** are listed in Table 2.

3.2. Crystallographic study

3.2.1. Crystal structure of complex 2 $[Co(valp)_2(2\text{-}ampy)_2]$

The crystal structure of complex **2** is shown in Fig. 1. The mononuclear $[Co(valp)_2(2\text{-}ampy)_2]$ complex crystallizes in triclinic crystal system and P-1 space group. For the four molecules per unit cell, the asymmetric unit (one molecule) consists of one Co(III) cation, two bidentate chelating valp groups and two monodentate 2-ampy ligands forming distorted octahedral geometry; (O(2)–Co(1)–O(1) = 59.5(2)°, O(1)–Co(1)–O(3) = 95.6(3)°, O(4)–Co(1)–O(3) = 103.5(3)°, O(4)–Co(1)–N(3) = 103.5(3)°, N(1)–Co(1)

Table 1
Crystallographic data and structure refinements for complex **2** and **3**.

	Complex 2		Complex 3	
Empirical formula	C_{26} H_{42} Co N_4 O_4		C_{50} H_{74} Co_2 N_2 O_8	
Formula weight	533.57		948.97	
Temperature	293(1) K		295(1) K	
Wavelength	0.71073 Å		0.71073 Å	
Crystal system	Triclinic		Orthorhombic	
Space group	P-1		Pbca	
Unit cell dimensions	a = 9.810(2) Å	α = 74.032(3)°	a = 20.541(3) Å	α = 90°
	b = 14.660(2) Å	β = 89.287(3)°	b = 11.247(1) Å	β = 90°
	c = 21.820(4) Å	γ = 84.123(3)°	c = 22.443(3) Å	γ = 90°
Volume	3000.5(8) $Å^3$		5184.7(1) $Å^3$	
Z	4		4	
Density (calculated)	1.181 Mg/m^3		1.216 Mg/m^3	
Absorption coefficient	0.606 mm^{-1}		0.690 mm^{-1}	
F(000)	1140		2024	
Crystal size	0.50 × 0.08 × 0.08 mm^3		0.55 × 0.21 × 0.11 mm^3	
Theta range for data collection	2.29–26.00°.		2.26–26.00°.	
Index ranges	$-12 \le h \le 12$, $-18 \le k \le 17$, $-26 \le l <= 26$		$-25 \le h \le 25$,$-13 \le k \le 13$, $27 \le l \le 27$	
Reflections collected	25036		48124	
Independent reflections	11567 [R(int) = 0.0835]		5070 [R(int) = 0.0882]	
Completeness to theta = 26.00°	98.3%		99.8%	
Absorption correction	Semi-empirical from equivalents		Semi-empirical from equivalents	
Max. and min. transmission	0.9531 and 0.7516		0.9280 and 0.7029	
Refinement method	Full-matrix least-squares on F^2		Full-matrix least-squares on F^2	
Data/restraints/parameters	11567/4/568		5070/4/214	
Goodness-of-fit on F^2	1.132		1.397	
Final R indices[a] [I > 2sigma(I)]	R1 = 0.1519, w*R2* = 0.3215		R1 = 0.2198, w*R2* = 0.4492	
R indices (all data)	R1 = 0.2611, w*R2* = 0.3809		R1 = 0.2352, w*R2* = 0.4579	
Largest diff. peak and hole	0.718 and −0.636 e.$Å^{-3}$		1.097 and −0.684 e.$Å^{-3}$	

[a] $R1 = \sum||Fo| - |Fc||/\sum|Fo|$ and $wR2 = \{\sum[w(Fo^2 - Fc^2)^2]/\sum[w(Fo^2)^2]\}^{1/2}$.

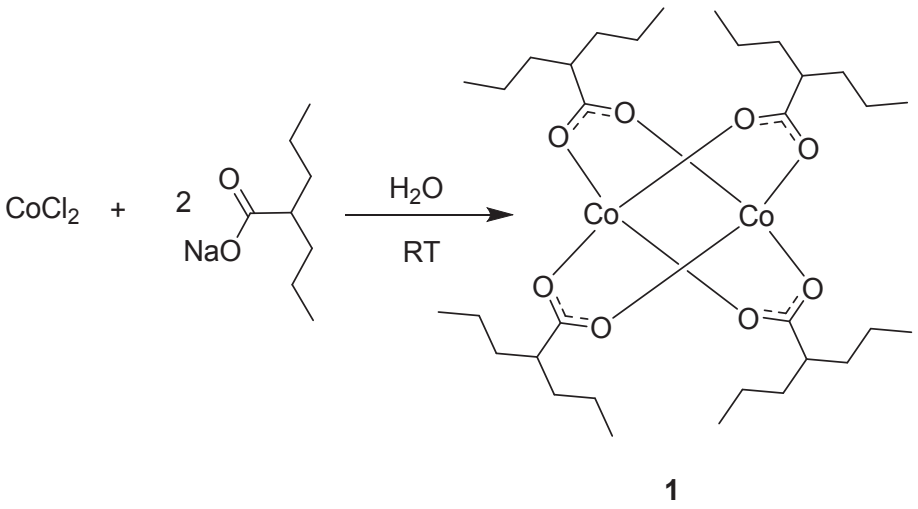

1

Scheme 1. Synthesis of $[Co_2(valp)_4]$ (**1**).

−N(3) = 96.5(3)°, O(2)−Co(1)−N(1) = 106.3(3)°). Selected bond distances (Å) and bond angles (°) for complex **2** are reported in Table 3.

The bond distances of Co−N and Co−O are ligand dependent, the average bond distances of Co−N (2.077 Å) and Co−O (2.189 Å) in complex **2** are longer than those found in [*cis*-Co(en)$_2$($C_8H_7O_2$)$_2$]($C_8H_7O_2 \cdot 2H_2O$) (1.945 Å) and (1.910 Å) respectively, where $C_8H_7O_2$ is *p*-methyl benzoate and en is ethylene diamine [35].

The N(1)−Co(1)−N(3) (96.5°) and O(1)−Co(1)−O(3) (95.6°) bond angles in complex **2** are shorter than the same angles found in [Zn(valp)$_2$(2-ampy)$_2$] complex (102.84°, 124.92°, respectively) [20].

Intramolecular hydrogen bonding within a molecule and intermolecular hydrogen bonding between molecules play a key role in the complex geometry and in stabilizing the complex in the solid state [9,36]. The hydrogen bonding in complex **2** are summarized in Table 4. The data show four intermolecular hydrogen bonding; (N(2)−H(2N2)···O(7)#2 = 2.22 Å, N(4)−H(2N4)···O(6) = 2.18 Å, N(6)−H(2N6)···O(3) = 2.19 Å and N(8)−H(2N8)···O(1)#1 = 2.12 Å) and two intramolecular hydrogen bonds (N(2)−H(1N2)···O(4) = 2.12 Å and N(4)−H(1N4)···O(2) = 2.10 Å).

3.2.2. Crystal structure of complex 3 [$Co_2(valp)_4(quin)_2$]

The crystal structure of complex **3** is shown in Fig. 2. The dinuclear [$Co_2(valp)_4(quin)_2$] complex crystallizes in orthorhombic crystal system and Pbca space group. For the four molecules per unit cell, the asymmetric unit (one molecule) consists of two Co cations, four valp and two quin molecules. Selected bond distances

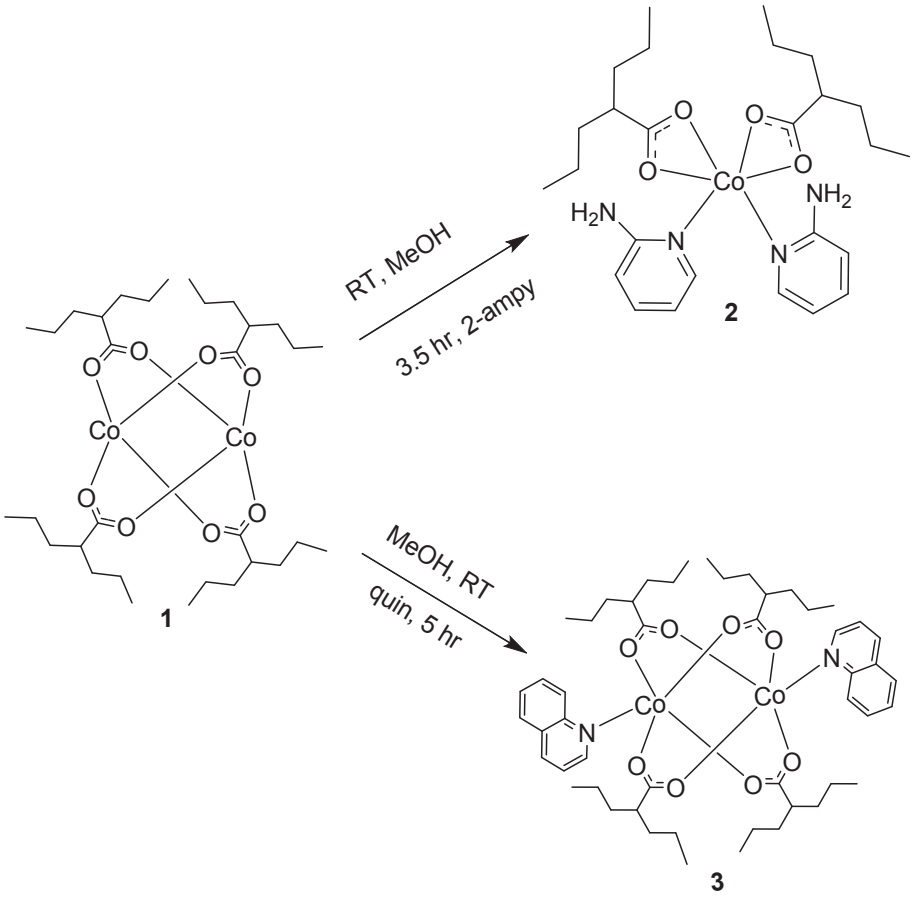

Scheme 2. Synthesis of complexes **2** and **3**.

Table 2
Physical properties and %yields of complexes **1**–**3**.

Complex	m.p (°C)	% Yield	Solubility
$Co_2(valp)_4$ (**1**)	58	86.50	CH_3OH, ether, petroleum ether
$Co(valp)_2(2\text{-ampy})_2$ (**2**)	121–125	79.85	CH_3OH, ether, CH_2Cl_2, CH_3CN, $(CH_3)_2CO$, C_2H_5OH, $CHCl_3$
$Co_2(valp)_4(quin)_2$ (**3**)	110–111	26.23	CH_3OH, ether, CH_2Cl_2, CH_3CN, $(CH_3)_2CO$, C_2H_5OH, $CHCl_3$

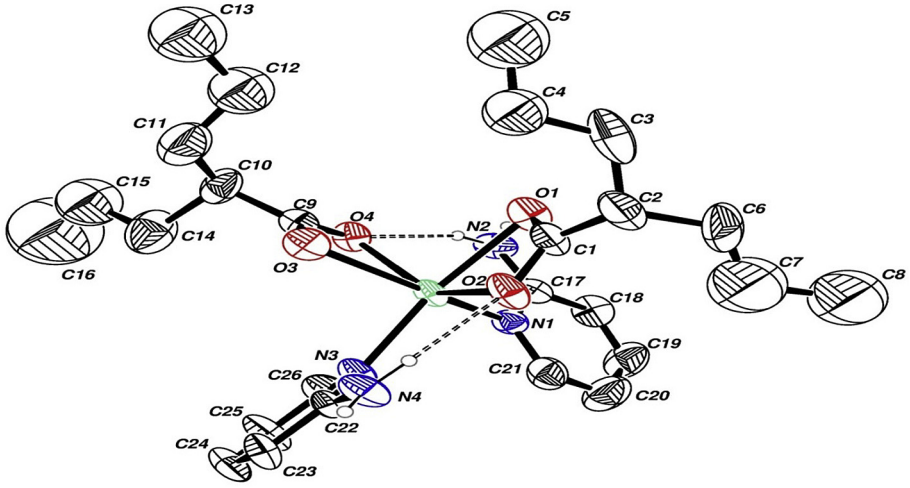

Fig. 1. X-ray structure of $Co(valp)_2(2\text{-ampy})_2$ (2).

Table 3
Selected bond distances (Å) and bond angles (°) for complex **2**.

Bond	Distance (Å)	Bonds	Angle (°)
Co(1)–N(1)	2.072(9)	O(2)–Co(1)–O(1)	59.5(2)
Co(1)–N(3)	2.081(8)	O(1)–Co(1)–O(3)	95.6(3)
Co(1)–O(1)	2.292(7)	O(2)–Co(1)–N(1)	106.3(3)
Co(1)–O(2)	2.053(7)	N(1)–Co(1)–N(3)	96.5(3)
Co(1)–O(3)	2.367(8)	O(4)–Co(1)–N(3)	103.5(3)
Co(1)–O(4)	2.042(7)	O(4)–Co(1)–O(3)	58.3(2)
C(9)–O(3)	1.233(11)	C(17)–N(1)–Co(1)	126.9(7)
C(9)–O(4)	1.264(10)	C(26)–N(3)–Co(1)	115.7(7)
C(22)–N(3)	1.353(11)	C(9)–O(4)–Co(1)	97.8(6)
C(26)–N(3)	1.341(14)	C(9)–O(3)–Co(1)	83.5(6)
C(17)–N(1)	1.362(11)	C(1)–O(1)–Co(1)	85.8(7)
C(21)–N(1)	1.324(14)	C(1)–O(2)–Co(1)	95.0(7)
C(1)–O(1)	1.217(12)	O(3)–C(9)–O(4)	120.4(11)
C(1)–O(2)	1.285(12)	O(1)–C(1)–O(2)	119.8(11)

Table 4
Hydrogen bonds in complex **2**.

D-H … A (Å)	d(D-H) (Å)	d(H … A) (Å)	d(D … A) (Å)	<(DHA) (°)
N(8)–H(2N8)···O(1)#1	0.86	2.12	2.921(9)	154.6
N(8)–H(1N8)···O(5)	0.86	2.10	2.925(10)	159.7
N(6)–H(2N6)···O(3)	0.86	2.19	2.984(10)	152.8
N(6)–H(1N6)···O(8)	0.86	2.15	2.980(11)	160.7
N(4)–H(2N4)···O(6)	0.86	2.18	3.009(10)	160.8
N(4)–H(1N4)···O(2)	0.86	2.10	2.931(11)	161.8
N(2)–H(1N2)···O(4)	0.86	2.12	2.947(11)	162.5
N(2)–H(2N2)···O(7)#2	0.86	2.22	3.019(10)	155.0

Symmetry transformations used to generate equivalent atoms: #1 x,y+1,z #2 x,y-1,z.

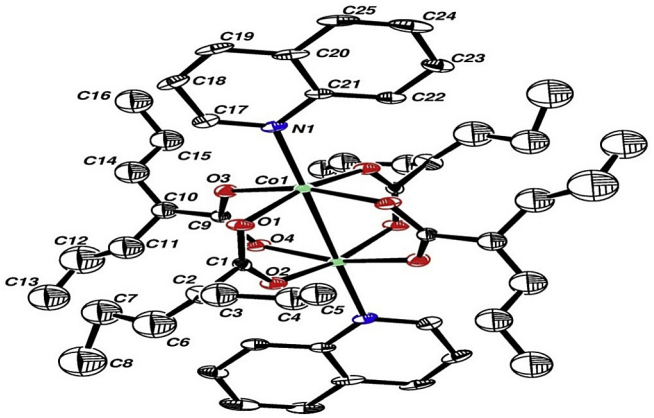

Fig. 2. X-ray structure of $Co_2(valp)_4$ $(quin)_2$ (3).

Table 5
Selected bond distances (Å) and bond angles (°) for complex **3**.

Bond	Distance (Å)	Bonds	Angle (°)
Co(1)–Co(1)#1	2.791(3)	O(1)–Co(1)–O(3)	86.7(4)
Co(1)–N(1)	2.106(9)	O(3)–Co(1)–N(1)	94.5(4)
Co(1)–O(3)	2.055(9)	O(2)#1-Co(1)–N(1)	97.9(4)
Co(1)–O(2)#1	2.037(9)	O(4)#1-Co(1)–N(1)	102.2(4)
Co(1)–O(1)	2.046(9)	O(3)–Co(1)–Co(1)#1	79.2(2)
O(2)–Co(1)#1	2.037(9)	O(1)–Co(1)–Co(1)#1	87.4(2)
O(4)–Co(1)#1	2.034(8)	C(17)–N(1)–Co(1)	114.1(9)
C(17)–N(1)	1.300(17)	C(1)–O(1)–Co(1)	117.4(8)
C(21)–N(1)	1.371(16)	C(9)–O(3)–Co(1)	127.8(8)
C(9)–O(3)	1.242(14)	N(1)–Co(1)–Co(1)#1	171.4(3)
C(9)–O(4)	1.245(13)	C(9)–O(4)–Co(1)#1	122.0(8)
C(1)–O(1)	1.225(13)	C(1)–O(2)–Co(1)#1	131.4(8)
C(1)–O(2)	1.249(13)	C(22)–C(21)–N(1)	120.7(11)

and bond angles for complex **3** are listed in Table 5.

The distorted octahedral geometry around each Co center consists of four oxygen atoms from four valproate bidentate chelating ligands and one nitrogen atom from quinoline monodentate ligand; O(1)–Co(1)–O(3) = 86.7(4)°, O(3)–Co(1)–N(1) = 94.5(4)°, O(2)#1-Co(1)–N(1) = 97.9(4)°, O(4)#1-Co(1)–N(1) = 102.2(4)°, O(3)–Co(1)–Co(1)#1 = 79.2(2)° and O(1)–Co(1)–Co(1)#1 = 87.4(2)°.

The (Co–Co) bounding distance is 2.791(3) Å which is shorter than Zn–Zn bond in $[Zn_2(valp)_4(quin)_2]$ (2.948(3) Å) [20]. The average bond distances of Co–O (2.043 Å) and Co–N (2.106 Å) are similar to previously reported values (2.07 Å and 2.090 Å, respectively) [37].

3.3. IR spectroscopy

The prepared cobalt complexes were characterized by measuring their IR spectra in the range of 200–4000 cm^{-1} as KBr disk. The IR spectral data for Na_{valp} [20,38–40] and complexes **1**–**3** are listed in Table 6. The IR spectra for complex **1** shows two carboxylate stretching bands asymmetric, $\nu_{as}(COO^-)$ at 1556 cm^{-1} and symmetric, $\nu_s(COO^-)$ at 1419 cm^{-1}. The difference between $\nu_{as}(COO^-)$ and $\nu_s(COO^-)$ is $\Delta\nu(COO^-)$ and its value (137 cm^{-1}) for complex **1** is the same as in Na_{valp} which may indicate bridging bidentate coordination mode between cobalt and the valproate carboxylic group [41,42].

For complex **2**, the $\nu_{as}(COO^-)$ at 1565 cm^{-1} and $\nu_s(COO^-)$ at 1448 cm^{-1} have been observed. The $\Delta\nu$ value for complexes **2** (117 cm^{-1}) is less than $\Delta\nu$ of Na_{valp} (137 cm^{-1}) which indicates bidentate chelating coordination mode.

However, in complex **3** the $\nu_{as}(COO^-)$ was observed at 1560 cm^{-1} and $\nu_s(COO^-)$ at 1450 cm^{-1}, $\Delta\nu$ (COO^-) = 110 cm^{-1} which is smaller than $\Delta\nu$ of Na_{valp} supporting a bidentate bridging coordination mode. Two primary amine NH absorption frequencies at $\nu_{as}(NH_2)$ = 3413 cm^{-1} and $\nu_{as}(NH_2)$ = 3331 cm^{-1} were also observed and suggest that the coordination mode with metal to be through the pyridine nitrogen atom as supported by its X-ray structure analysis.

3.4. Magnetic moments and UV–Vis spectral data for cobalt complexes

The electronic spectra of cobalt complexes were recorded in MeOH solution. The electronic transition data for complexes **1**–**3** and their parent ligands are summarized in Table 7.

The magnetic moment of complex **2** was determined and calculated by using the spin only formula. Table 8 shows the magnetic properties for complex **2**. On the other hand, the magnetic moments for complexes **1** and **3** couldn't be measured due to unsuccessful packing process.

The electronic spectrum of complex **1** exhibits two bands. The band at 270 nm (7576.5 L mol^{-1} cm^{-1}) was assigned to the charge transfer band with extinction coefficients larger than 1000 L mol^{-1} cm^{-1} whereas the band at 492 nm (43.55 L mol^{-1} cm^{-1}) was assigned to the cobalt DMSO-d_6

Table 6
Assignment of IR bands and wave numbers for Na_{valp} and **1**–**3** complexes.

Assignments	Na_{valp} (cm^{-1})	Complex 1 (cm^{-1})	Complex 2 (cm^{-1})	Complex 3 (cm^{-1})
$\nu_{as}(COO^-)$	1548	1556	1565	1560
$\nu_s(COO^-)$	1411	1419	1448	1450
$\Delta\nu(COO^-)$	137	137	117	110
ν_{as}(N-H)	–	–	3413	–
ν_s(N-H)			3331	

Table 7
The electronic data for **1**–**3** complexes and their parent ligands.

Complex	λ_{max} (nm)	ϵ (L mol^{-1} cm^{-1})	Pure ligands	λ_{max} (nm)	ϵ (L mol^{-1} cm^{-1})
$Co_2(valp)_4$ (**1**)	270	7576.5	–	–	–
	492	43.55			
$Co(valp)_2(2\text{-ampy})_2$ (**2**)	235	20072	2-ampy	234	11479
	295	8022.1		291	5569.5
	520	20.2			
$Co_2(valp)_4(quin)_2$ (**3**)	213	49030	Quin	204	44107
	276	9119		225	41442
	366	3.6		276	3605.9
	520	2.6			

Table 8
Magnetic properties for complex **2**.

Complex	Magnetic moments (μ_{eff}) (BM)	# of unpaired electrons (n)
$Co(valp)_2$ $(2\text{-ampy})_2$ (**2**)	4.83	4

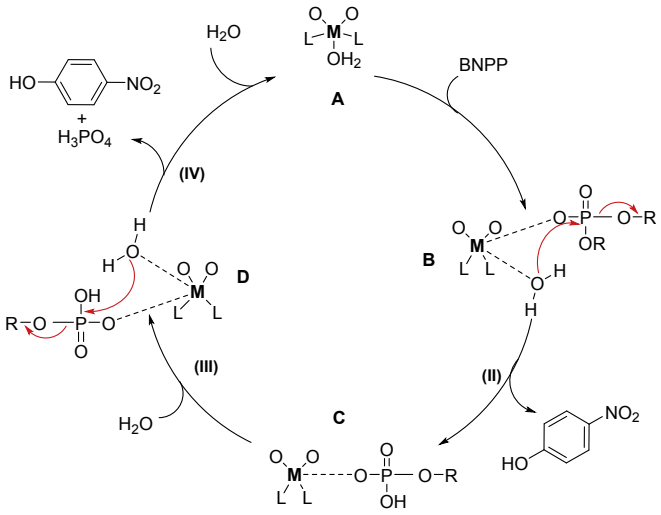

Fig. 3. The possible mechanism of the BNPP catalytic cleavage.

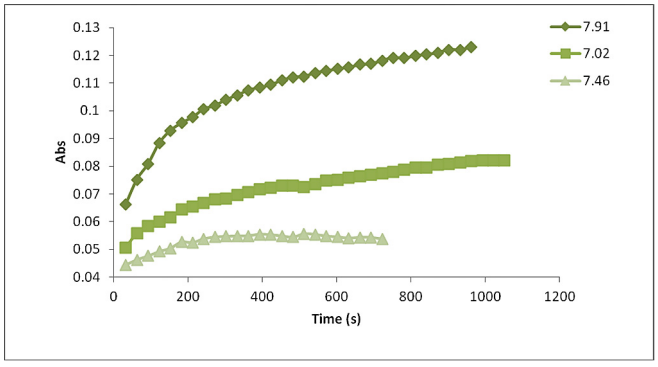

Fig. 4. BNPP hydrolysis by complex 3 in MeOH/HEPEs buffer solution with different pH values under the selected conditions (T = 37 °C, [complex 3] = 2 × 10^{-3} M and [BNPP] = 1 × 10^{-4} M).

transition [43].

The bands between 213 and 295 nm for complexes **2** and **3** were assigned to the intra-ligand transition bands in addition to charge transfer bands. The results also showed similarities between the cobalt complexes and their parent ligands and complex **1** with very small shifts caused by Co coordination.

The magnetic moment of complex **2** is 4.50 BM. This value indicates the presence of four unpaired electrons supporting a high spin d^6 octahedral geometry. The electronic spectrum of this complex exhibits one DMSO-d_6 transition band (520 nm). Moreover, high spin Co(III) octahedral complex **2** was obtained because 2-ampy ligand in the present case behaved as weak field ligand [44].

The electronic spectrum of complex **3** exhibits two DMSO-d_6 transition bands at 366 nm (3.6 L mol^{-1} ^{1}cm^{-1}) and 520 nm (2.6 L mol^{-1} cm^{-1}) for complex **3** as a result of $^4T_{1g} \rightarrow {}^4T_{2g}(F)$ and $^4T_{1g} \rightarrow {}^4T_{1g}(P)$ electronic transition bands. The third band ($^4T_{1g} \rightarrow {}^4A_{2g}(F)$) is embedded in the charge transfer bands and intra-ligand transition bands. The UV–Vis spectral data for complexes **3** is similar to those observed for $[Co(2\text{-ampy})_2(dca)_2]$ [8,45].

3.5. BNPP catalytic hydrolysis

The rate of BNPP hydrolysis was studied at different

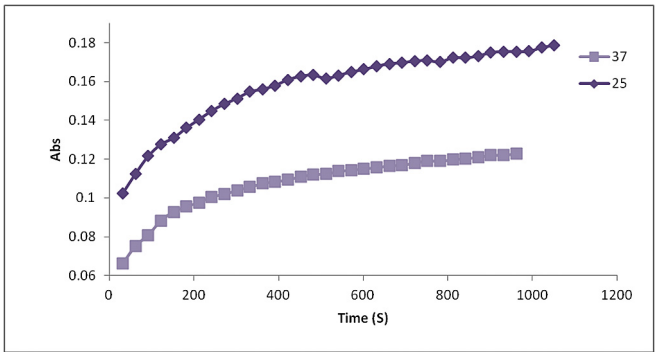

Fig. 5. BNPP hydrolysis by complex 3 in MeOH/HEPEs buffer solution with different temp values under the selected conditions (pH = 7.91, [complex 3] = 2 × 10^{-3} M and [BNPP] = 1 × 10^{-4} M).

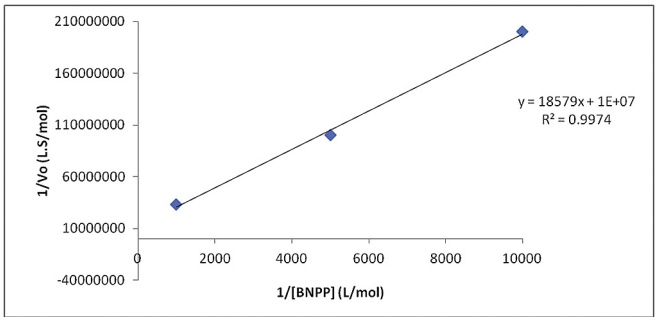

Fig. 6. Second order rate for complex 2 with different [BNPP] under the selected conditions (pH = 7.91, temp = 25 °C and [complex 2] = 2 × 10^{-4} M).

Table 9
Kinetic parameters of the phosphate diester group hydrolysis for complexes **2** and **3** at different BNPP concentrations.

Concentration(M)		V_o (mol/L s)	V_{max} (mol/L s)	K_m (mol/L)	K_{cat}[a] (s^{-1})	2nd-order rate K_{BNPP}[b] (L mol^{-1} s^{-1})
Complexes	BNPP					
2 (2×10^{-4})	1×10^{-3}	3.0×10^{-8}	1×10^{-7}	1.9×10^{-3}	5×10^{-4}	2.60×10^{-1}
2 (2×10^{-4})	2×10^{-4}	1.0×10^{-8}				
2 (2×10^{-4})	1×10^{-4}	5.0×10^{-9}				
3 (2×10^{-6})	1×10^{-3}	1.0×10^{-8}	1.0×10^{-8}	6.5×10^{-6}	5×10^{-3}	7.70×10^{2}
3 (2×10^{-6})	1×10^{-4}	9.0×10^{-9}				
3 (2×10^{-6})	1×10^{-5}	6.0×10^{-9}				

[a] $K_{cat} = V_{max}/[complex]$.
[b] $K_{BNPP} = K_{cat}/K_m$.

temperatures, pH and concentrations. The optimum condition for BNPP hydrolysis was obtained by changing one of the above factors while maintaining the other two constant. All cobalt valproate complexes were used as catalysts. One possible mechanism of the BNPP catalytic cleavage is shown in Fig. 3.

3.5.1. Effect of pH on BNPP catalytic hydrolysis

The pH value of 7.46 was selected in close agreement with the physiological pH value. For comparison purposes, a lower value and a higher value of pH values were selected for further experimentation.

Fig. 4 shows the Abs versus time relationship for complex **3** at different pH values and constant temp and concentration of both BNPP and complex. The initial rate (V_o) of BNPP hydrolysis was calculated by measuring the absorbance of p-nitrophenol against time at 400 nm [32,33]. The V_o values (mol/L.S) are 1×10^{-8}, 3×10^{-9} and 5×10^{-9} at pH = 7.91, 7.46 and 7.02, respectively for complex **3**. The maximum V_o was obtained at pH = 7.91 for complex **3**.

3.5.2. Effect of temperature on the BNPP catalytic hydrolysis

Fig. 5 shows the Abs versus time relationship for complex **3** at different temp values and constant pH and concentration of both BNPP and complex. The V_o values (mol/L.S) are 1.8×10^{-8} and 1.7×10^{-8} at 25 °C and 37 °C for complex **3**. The maximum V_o was obtained at 25 °C for complex **3**.

Complexes **2** and **3** showed similar trend in the hydrolysis of BNPP. The hydrolysis of BNPP has been analyzed by using Michaelis–Menten equation [46] ($1/V_o = 1/V_{max} + K_m/V_{max}[BNPP]$) (Fig. 6).

The Kinetic parameters of BNPP hydrolysis are shown in Table 9. The results from this study showed that the rate of BNPP hydrolysis by the prepared complexes was in the following order: **3** > **2** and their values are higher than other synthetic chemical models (K_{cat}/K_m = 1.3–43 × 10^{-5} M^{-1} s^{-1} at 35 °C and pH 7.3–10.5 for Zn complexes) [46]. Complex **3** showed the highest activity due to its dimmer complex.

4. Conclusion

The new cobalt complexes with valproate in the presence of N-donor ligands were fully characterized by IR, UV–Vis spectrophotometric methods and single crystal X-ray crystallography. The synthesized complexes were $[Co_2(valp)_4]$ **(1)**, $[Co(valp)_2(2\text{-ampy})_2]$ **(2)** and $[Co_2(valp)_4(quin)_2]$ **(3)**.

The structure of **2** revealed distorted octahedral geometry with two bidentate valp groups and two monodentate 2-ampy ligands. In complex **3**, the distorted octahedral geometry around each Co center of the binuclear complex consists of four oxygen atoms from four valproate bidentate chelating ligands and one nitrogen atom from quinoline monodentate ligand.

The rate of BNPP hydrolysis was studied by UV–Vis spectrophotometric method in order to determine the effect of cobalt complexes on the phosphatase hydrolysis. The results showed that the hydrolysis rate of BNPP was 7.70×10^2 L mol^{-1} s^{-1} for (**3**) and 2.60×10^{-1} L mol^{-1} s^{-1} for (**2**) and their values are higher than other synthetic chemical models.

Acknowledgment

The authors thank the Office of Vice President for Academic Affairs at Birzeit University for their financial support.

Appendix A. Supplementary data

CCDC **1488000** and **1488002** contain the supplementary crystallographic data for **2** and **3**, respectively. These data can be obtained free of charge via http://www.ccdc.cam.ac.uk/conts/retrieving.html, or from the Cambridge Crystallographic Data Center, 12 Union Road, Cambridge CB2 1EZ, UK; fax: (+44) 1223-336-033; or e-mail: deposit@ccdc.cam.ac.uk. Supplementary data associated with this article can be found, in the online version, at http:// …

References

[1] M. Agwara1, P. Ndifon, P. Ndosiri, N. Ndosiri, A. Paboudam, D. Yufanyi, A. Mohamadou, Chem. Soc. Ethiop. 24 (3) (2010) 383–389.
[2] R.H. Abeles, D. Dolphin, Acc. Chem. Res. 1975 (259) (1971) 114–120.
[3] E.L. Chang, C. Simmers, D.A. Knight, Pharmaceuticals 3 (6) (2010) 1711–1728.
[4] F. O'Leary, S. Samman, Nutrients 2 (3) (2010) 299–316.
[5] X. Fan, J. Dong, R. Min, Y. Chen, X. Yi, J. Zhou, S. Zhang, J. Coord. Chem. 66 (24) (2013) 4268–4279.
[6] M.C. Heffern, N. Yamamoto, R.J. Holbrook, A.L. Eckermann, T.J. Meade, Curr. Opin. Chem. Biol. 17 (2) (2014) 189–196.
[7] M. Vlasiou, EC Chem. 2 (2015) 35–47.
[8] A. Colette, B. Yuoh, M.O. Agwara, D.M. Yufanyi, M.A. Conde, R. Jagan, K.O. Eyong, Int. J. Inorg. Chem. (2015) 9–12.
[9] L. Kucková, K. Jomová, A. Švorcová, M. Valko, P. Segľa, J. Moncoľ, J. Kožíšek, Molecules 20 (2) (2015) 2115–2137.
[10] a) H. Abu Ali, H. Fares, M. Darawsheh, E. Rappocciolo, M. Akkawi, S. Jaber, Eur. J. Med. Chem. 89 (2015) 67;
b) H. Abu Ali, S.N. Omar, M.D. Darawsheh, H. Fares, J. Coord. Chem. 69 (2016) 1110;
c) B. Jabali, H. Abu Ali, Polyhedron 117 (2016) 249;
d) H. Abu Ali, S. Maloul, I. Abu Ali, M. Akkawi, S. Jaber, J. Coord. Chem. 69 (2016) 2514;
e) H. Abu Ali, A. Shalash, M. Akkawi, S. Jaber, Appl. Organomet. Chem. (2017), http://dx.doi.org/10.1002/aoc.3772;
f) H. Abu Ali, S. Kamel, A. Abu Shamma, Appl. Organomet. Chem. (2017), http://dx.doi.org/10.1002/aoc.3829.
[11] Z. Jaman, M.R. Karim, T.A. Siddiquee, A.H. Mirza, M.A. Ali, Int. J. Org. Chem. 3 (2013) 214–219.
[12] S.D. Dhumwad, J. Chem. Pharm. Res. 3 (4) (2011) 504–517.
[13] G.K. Belin, S. Krähenbühl, P.C. Hauser, J. Chromatogr. B Anal. Technol. Biomed. Life Sci. 847 (2) (2007) 205–209.
[14] C.M.X. José, C.L.V. Emilio, da G. N.-M. Maria, S.de B.V. Glauce, Neurosci. Med. 3 (01) (2012) 107–123.
[15] M.F. Silva, C.C. Aires, P.B. Luis, J.P. Ruiter, L. I. J., M. Duran, R.J. Wanders, I. Tavares de Almeida, J. Inherit. Metab. Dis. 31 (2) (2008) 205–216.
[16] S. Beatriz, R. Fagundes, Rev. Neurocienc. 16 (2) (2008) 130–136.
[17] M. Kostrouchová, Z. Kostrouch, M. Kostrouchová, Folia Biol. (Praha). 53 (2)

(2007) 37–49.
[18] http://www.spotidoc.com/doc/153438/carbamazepinetegretol-organization-of-teratology-info pdf. (Accessed 20 January 2016).
[19] T.K. Todorova, F. Poineau, P.M. Forster, L. Gagliardi, K.R. Czerwinski, A.P. Sattelberger, Polyhedron 70 (2014) 144–147.
[20] M. Darawsheh, H. Abu Ali, A.L. Abuhijleh, E. Rappocciolo, M. Akkawi, S. Jaber, S. Maloul, Y. Hussein, Eur. J. Med. Chem. 82 (2014) 152–163.
[21] A. Abuhijleh, C. Woods, J. Inorg. Biochem. 64 (1) (1996) 55–67.
[22] H. Abu Ali, M.D. Darawsheh, E. Rappocciolo, Polyhedron 61 (2013) 235–241.
[23] L. Tabrizi, P. Mcardle, M. Ektefan, H. Chiniforoshan, Inorg. Chim. Acta 439 (2016) 138–144.
[24] K. Dong, M. Xiang-Guang, J. Du Ying Liu, K. Xing-Ming, Z. Xian-Cheng, Physiochem. Eng. Asp. 324 (2008) 189–193.
[25] W. Jiang, B. Xu, J. Zhong, J. Li, F. Liu, J. Chem. Sci. 120 (4) (2008) 411–417.
[26] J. Li, H. Li, B. Zhou, W. Zeng, S. Qin, S. Li, J. Xie, Transit. Met. Chem. 30 (3) (2005) 278–284.
[27] J. Xie, C. Li, B. Wang Jiang, Chem. Pap. 67 (4) (2013) 365–371.
[28] K. Hasegawa, Rigaku J. 28 (1) (2012) 14–18.
[29] SHELXTL-NT V6.1, BRUKER AXS GMBH, D-76181 Karlsruhe, Germany, 2002.
[30] SMART-NT V5.6, Bruker AXS GMBH, D-76181 Karlsruhe, Germany, 2002.
[31] J. Torres, M. Brusoni, F. Peluffo, C. Kremer, S. Domínguez, A. Mederos, E. Kremer, Inorg. Chim. Acta 358 (12) (2005) 3320–3328.
[32] A. Shalash, H. Abu Ali, Faculty of Graduate Studies Non-steroidal Zn(II) and Co(II) Sulindac Drugs and Bioactive Bacterial Effect, Anti-malarial Effect and the Use as Phosphate Hydrolyzing Enzymes, Birzeit University, 2015.
[33] A. Abuhijleh, Polyhedron 16 (4) (1997) 733–740.
[34] J. Li, H. Li, B. Zhou, W. Zeng, S. Qin, S. Li, J. Xie, Transit. Met. Chem. 30 (2005) 278–284.
[35] R. Sharma, R.P. Sharma, R. Bala, M. Quirós, J.M. Salas, Inorg. Chem. Commun. 9 (11) (2006) 1075–1078.
[36] H. Abu Ali, B. Jabali, Polyhedron 107 (2015) 97–106.
[37] E. Bugella-altamirano, J.M. Gonza, Polyhedron 19 (2000) 2473–2481.
[38] http://www.pmda.go.jp/files/000152839.pdf (Accessed 8 February 2016).
[39] I.A. Alsarra, M. Al-Omar, F. Belal, Profiles Drug Subst. Excipients Relat. Methodol. 32 (05) (2005) 209–240.
[40] Z.L. Chang, Sodium Valproate and Valproic Acid, vol. 8, Academic Rcss, Inc., 1979.
[41] C.C.R. Sutton, G. da Silva, G.V. Franks, Chem. Eur. J. 21 (2015) 6801–6805.
[42] P. Nelson, R. Taylor, Appl. Petrochem Res. 4 (2014) 253–285.
[43] A.B.P. Lever, J. Chem. Educ. 51 (9) (1974) 612–616.
[44] J. Wiley, S. Ltd, A. Blackman, Encycl. Inorg. Chem. (2006) 1–25.
[45] N.H. Al-Shaalan, Molecules 16 (10) (2011) 8629–8645.
[46] A. Ercan, H.I. Park, L.-J. Ming, Chem. Commun. 24 (2000) 2501–2502.